Nanoscale

PAPER

View Article Online
View Journal

Cite this: DOI: 10.1039/c4nr06461e

Highly stable piezo-immunoglobulin-biosensing of a SiO_2/ZnO nanogenerator as a self-powered/active biosensor arising from the field effect influenced piezoelectric screening effect

Yayu Zhao, Yongming Fu, Penglei Wang, Lili Xing* and Xinyu Xue*

Received 3rd November 2014,
Accepted 7th December 2014

DOI: 10.1039/c4nr06461e

www.rsc.org/nanoscale

Highly stable piezo-immunoglobulin-biosensing has been realized from a SiO_2/ZnO nanowire (NW) nanogenerator (NG) as a self-powered/active biosensor. The piezoelectric output generated by the SiO_2/ZnO NW NG can act not only as a power source for driving the device, but also as a sensing signal for detecting immunoglobulin G (IgG). The stability of the device is very high, and the relative standard deviation (RSD) ranges from 1.20% to 4.20%. The limit of detection (LOD) of IgG on the device can reach 5.7 ng mL^{-1}. The response of the device is in a linear relationship with IgG concentration. The biosensing performance of SiO_2/ZnO NWs is much higher than that of bare ZnO NWs. A SiO_2 layer uniformly coated on the surface of the ZnO NW acts as the gate insulation layer, which increases mechanical robustness and protects it from the electrical leakages and short circuits. The IgG biomolecules modified on the surface of the SiO_2/ZnO NW act as a gate potential, and the field effect can influence the surface electron density of ZnO NWs, which varies the screening effect of free-carriers on the piezoelectric output. The present results demonstrate a feasible approach for a highly stable self-powered/active biosensor.

Introduction

Biosensors have many applications in medical science, biological engineering, food industry, environmental monitoring and in the military.[1–5] Recently, world-wide research efforts have been made to fabricate high performance biosensors with high sensitivity, selectivity and stability.[6–9] ZnO nanowires (NWs) used for biosensing have been intensively investigated because of their biologically-friendly applications and low cost.[10–12] Additionally, ZnO NWs with wurtzite structures have high piezoelectric output under externally applied deformation, and a ZnO NW piezoelectric nanogenerator (NG) has been integrated in various self-powered nanosystems.[13–16] By coupling the piezoelectric and biosensing characteristics of ZnO NWs, a new type of biosensor can be realized through treating the piezoelectric output from the ZnO NW NG as both the power source and the biosensing signal.[17] The adsorption of biomolecules on the surface of ZnO NWs can modify the surface free-carrier density of the NWs, which can vary the screening effect of free-carriers on the piezoelectric output. Although the device and the piezo-biosensing mechanism are new, the biosensing performance is not high. The stability and the limit of detection (LOD) need to be improved for practical applications. For traditional NW-based biosensors, the field effect transistor (FET) structure has been found to be a good candidate for a highly stable biosensing device, which depends on the conductivity change of the NWs as biochemical species being adsorbed on the surface.[18] Thus, if the field effect can be introduced into the piezo-biosensing, then high stability can probably be realized. At the same time, a novel biosensing mechanism that combines piezoelectric effects, bisosensing characteristics and field effects can be established.

In this paper, highly stable piezo-IgG (immunoglobulin G) biosensing has been realized from the SiO_2/ZnO NW NG as a self-powered/active biosensor. A SiO_2 layer uniformly coated on the surface of the ZnO NW acts as the gate insulation layer, which increases mechanical robustness and protects it from the electrical leakages and short circuits. The positively charged IgG modified on the surface of the SiO_2/ZnO NW acts as the gate potential, and this field effect can influence the surface electron density of ZnO NWs, which varies the screening effect of free-carriers on the piezoelectric output. Our study can stimulate a research trend on designing a new device structure and exploring the mechanism for self-powered/active biosensors.

College of Sciences, Northeastern University, Shenyang 110004, China.
E-mail: xuexinyu@mail.neu.edu.cn, xinglili@mail.neu.edu.cn

Experimental

All chemicals (purchased from Sinopharm Chemical Reagent Co. Ltd) were analytical-grade reagents and used as purchased without further purification. Vertically-aligned ZnO NW arrays were synthesized by a wet-chemical method.[19] Prior to growth, a piece of Ti foil (thickness, 0.1 mm) as the substrate was cleaned with deionized water and alcohol, and dried at 60 °C (Fig. 1a). 0.416 g of zinc nitrate hexahydrate was dissolved in 38 mL of deionized water, stirred for 10 min at room temperature. After that, 2 mL of aqueous ammonia was added into the solution dropwise under continuous stirring. Then the Ti foil was immersed into the solution, and the reaction flask was sealed and kept at 70 °C for 24 hours. After cooling to the room temperature, the substrate coated with vertically-aligned ZnO NW arrays was removed from the solution, washed with deionized water, and dried at 60 °C (Fig. 1b). A thin SiO_2 layer was uniformly coated on ZnO NW arrays by a wet-chemical method. The substrate with ZnO NW arrays were placed into a mixture of isopropyl alcohol (35 mL), deionized water (0.4 mL), aqueous ammonia (0.1 mL), and tetraethoxysilane (0.025 mL). After magnetically stirring for 3 hours, the substrate was taken out, washed with deionized water/alcohol, and dried at 60 °C (Fig. 1c).

The crystal phase of the nanocomposites was characterized by X-ray powder diffraction (XRD; D/max 2500 V, Cu Kα radiation, λ = 1.5405 Å). The morphology and microstructure of the nanocomposites were investigated by using a scanning electron microscope (SEM, Hitachi S4800) with an energy dispersive X-ray spectrometer (EDS) and a transmission electron microscope (TEM, JEOL JEM-2100F), respectively.

The surface of SiO_2/ZnO NWs was modified with gold nanoparticle–anti-Immunoglobulin G (Au NP–anti-IgG) conjugates. Colloidal Au has been recognized as a versatile and efficient template for the immobilization of biomolecules due to its easy preparation, relatively large surface and good biocompatibility.[20,21] The colloidal Au can not only enhance the amount of antibodies immobilized on the surface of ZnO NWs, but also can preserve the activity of the immobilized biomolecules. Anti-IgG molecules were anchored to the surface of the SiO_2/ZnO NW through Au NPs.[22] 0.01 mL of Au NP–anti-IgG colloidal solution was added to the SiO_2/ZnO NW arrays, and then incubated in the fume hood for 1 hour. After that, the sample was treated with blocking buffer (BB) (0.1% Tween 20, 0.1% fish gelatin, and 1% bovine serum albumin (BSA). It was reported that BB could efficiently block the nonspecific binding of IgG to the samples.[22] Thus, treating the sample with BB can effectively diminish the undesirable response from the nonspecific binding to the sample and it is necessary for the specific function of the sensor. Samples treated by BB were dried at room temperature for 2 hours, and then cleaned with phosphate buffer solution (PBS).[23]

The device was composed of three major parts: SiO_2/ZnO NW arrays (after bio-functionalization) as the sensing material, Ti and Al foils as the electrodes, and Kapton film as the frame (Fig. 1d). The Ti foil acted as both the substrate for SiO_2/ZnO NW arrays and a conducting electrode. A piece of Al foil (thickness, 0.05 mm) positioned on the top of NW arrays acted as the counter-electrode. Two copper conducting leads were glued with silver paste on the two electrodes, respectively. After that, the device was tightly fixed between two sheets of a flexible Kapton board as the support frames to ensure the electric contact between the aluminum foil and the NWs. It has been confirmed that flexible Kapton layers as substrates can follow the height profiles of the NW arrays and make effective contacts between the tips of NWs and electrodes.[24] When detecting IgG, the device is immersed in a certain concentration of IgG for 1 hour to bind IgG molecules on the antibody. The device is rinsed with PBS and dried at room temperature. The device structure and the *ex-situ* measurement lead to the relatively long binding time. For future practical applications of self-powered biosensors, new device structures and new measurement types need to be developed to shorten the binding time of IgG molecules. Then the device was tested by an outside circuit and the data were collected by a computer (Fig. 1e). Under an applied force, the piezoelectric output of the device can act as both the power source and the biosensing signal. The hammer is controlled by a programed motor, and the area of the hammer for applying the compressive force is larger than that of the device. Thus the hammer can provide a stable and uniform force on the self-powered device for the experimental measurement. While testing, the two electrodes of the device are connected to a low-noise preamplifier (Model SR560, Stanford Research Systems) through coaxial lines. The data were collected by a computer through a data acquisition card.

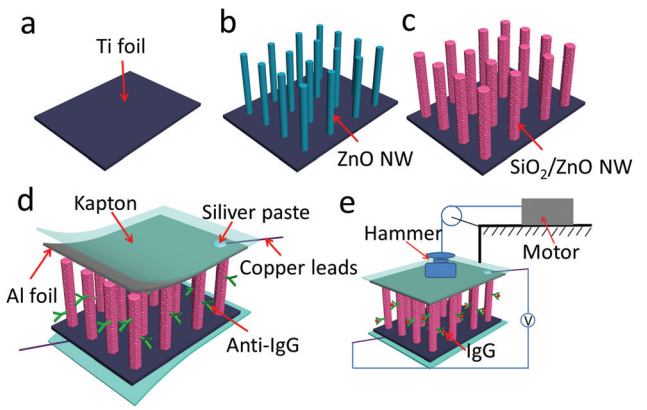

Fig. 1 Fabrication of the self-powered/active biosensor. (a) A pre-cleaned Ti foil is used as the substrate. (b) Vertically-aligned ZnO NW arrays are grown on the Ti foil. (c) SiO_2 layer is uniformly coated on the whole surface of ZnO NW arrays. (d) The structure design of the self-powered/active biosensor after the anti-IgG being assembled onto the surface of SiO_2/ZnO NWs. (e) Schematic image showing the measurement of the self-powered/active IgG sensing.

Results and discussion

Fig. 2a is a typical SEM image of SiO_2/ZnO NW arrays from the top view, showing that SiO_2/ZnO NW arrays are grown on the

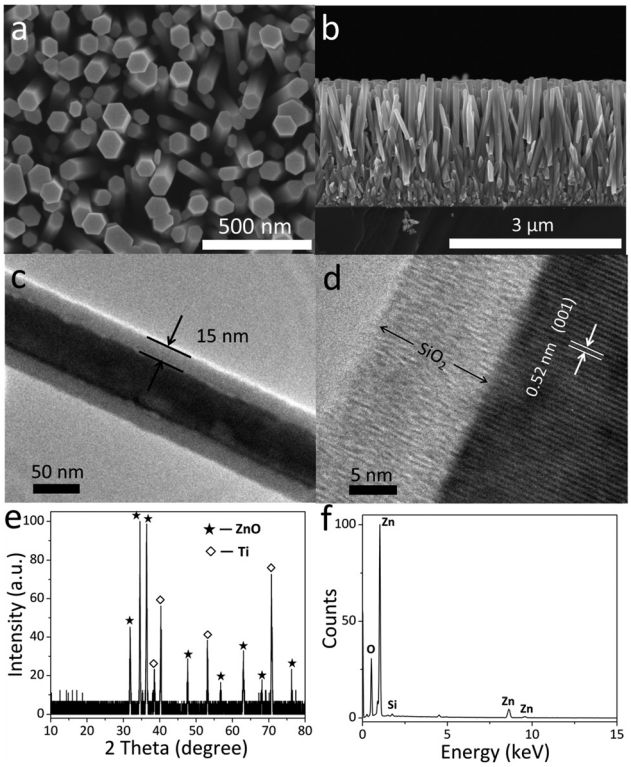

Fig. 2 (a) SEM image of SiO_2/ZnO NW arrays on the top view. (b) SEM image of SiO_2/ZnO NW arrays on the side view. (c) TEM image of SiO_2/ZnO NW. (d) HRTEM image of SiO_2/ZnO NW. (e) XRD pattern of SiO_2/ZnO NW arrays. (f) EDS spectra of SiO_2/ZnO NW arrays.

Ti substrate along a consistent growth direction. The average diameter of SiO_2/ZnO NWs is about 100 nm. The SEM image of SiO_2/ZnO NW arrays from the side view is shown in Fig. 2b, revealing that the nanoarrays have an average length of about 2.2 μm. It further confirms that SiO_2/ZnO NWs are vertically aligned on the substrate. Fig. 2c is the TEM image of one single SiO_2/ZnO NW, it can be seen that the whole surface of the ZnO NW is uniformly coated with a layer of SiO_2 (the thickness is about 15 nm). Fig. 2d is a high-resolution TEM (HRTEM) image of the SiO_2/ZnO NW, the lattice spacing of 0.52 nm corresponds to the (001) plane of hexagonal wurtzite ZnO. The XRD pattern of SiO_2/ZnO NW arrays is shown in Fig. 2e, and the sharp diffraction peaks indicate good crystalline quality. The peaks marked by stars can be indexed to ZnO (JCPDS file No. 36-1451), and the peaks marked by diamond can be indexed to Ti (JCPDS file No. 44-1294) arising from the Ti foil substrate. The peaks of SiO_2 were not observed in this XRD pattern, which can be explained by considering that the quantity of SiO_2 is much smaller than that of ZnO. Fig. 2f shows the EDS spectra of SiO_2/ZnO NW arrays. It can be seen that three elements (O, Zn, and Si) exist in the sample.

It is well known that ZnO NWs have a high density of point defect (oxygen vacancies), which provide n-type carriers (electrons) for their conductivity.[25,26] And ZnO NWs have high piezoelectric output under applied deformation, in which the piezoelectric polarization charges created by the strain of *c*-axis can drive electrons in the outside circuit transport. At the same time, the free electrons inside ZnO NWs can also have directional movement to partially screen the piezoelectric polarization charges in the NWs, and thereby the piezoelectric output voltage of NGs is lowered (piezoelectric screening effect).[27,28] The piezoelectric output of the ZnO NG is largely influenced by the carrier density inside ZnO NWs through the piezoelectric screening effect.[29] For example, after annealing in oxygen, ZnO NWs have fewer surface defects, resulting in less n-type carriers within ZnO NWs; the screening effect of the free carriers on the piezoelectric polarization charges is weak, thus the output of the ZnO NG is high.[30] Our previous work on the self-powered/active biosensing of ZnO NWs has shown that positively charged IgG anchored on the surface can change the free-carrier density at the surfaces of ZnO NWs, thus affecting the piezoelectric output through the changes of the screening effect.[17] In this work, a layer of SiO_2 coated on the surface of ZnO NWs acts as a gate insulation layer and stabilizes the signal. In this case, Au nanoparticles, the insulating SiO_2 layer and semiconducting ZnO nanowires construct a simple MIS structure. The positively charged IgG acting as the gate electrode can modulate the carrier density of the conducting channel. When modified with different concentrations of IgG, a SiO_2/ZnO NG has a different piezoelectric screening effect, resulting in the change of piezoelectric outputs. The detailed work mechanism is as follows.

The detailed working mechanism of a SiO_2/ZnO-based self-powered/active biosensor driven by a compressive strain is shown in Fig. 3. As shown in Fig. 3a and b, SiO_2/ZnO NWs modified with Au NP–anti-IgG have not been functionalized with IgG molecules. Without any compressive force, the device is in the natural state without any piezoelectric output (Fig. 3a). The ZnO NWs are coated with an insulating layer, which increases mechanical robustness and protects it from the electrical leakages and short circuits that could occur

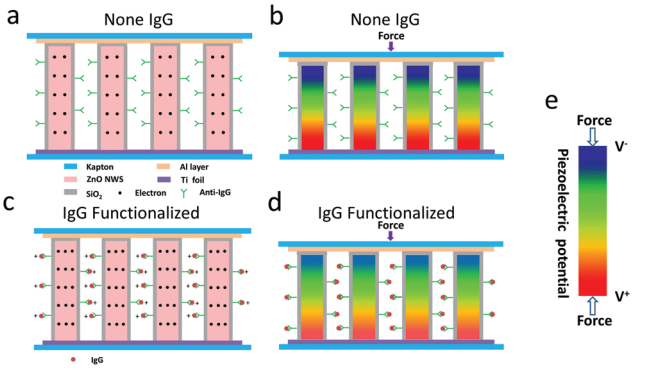

Fig. 3 The working mechanism of a SiO_2/ZnO-based self-powered/active biosensor. (a) The device (not modified with IgG molecules) without a compressive force. (b) The piezoelectric output of the device (not modified with IgG molecules) under a compressive force. (c) The device (modified with IgG molecules) without a compressive force. (d) The piezoelectric output of the device (modified with IgG molecules) under a compressive force. (e) The color scale bar representing the different piezoelectric potential.

because of the n-type non intentional doping of the as-grown ZnO NW. The top and bottom electrodes are used to collect electrical charges. In practice, the substrate can be readily used as the bottom electrode. When an external compressive force is applied on the device (Fig. 3b), the deformation of *c*-axis of ZnO NWs can lead to a piezopotential distribution along the ZnO NWs.[31,32] These piezoelectric polarization charges induce charges in the electrodes through electrons flowing in the external load from one electrode to the other for balancing the piezoelectric field. The dynamic potential drop across the top and bottom electrodes is the driving force for the transient flow of electrons in the external load in responding to the repeated mechanical deformation. At the same time, under the driving force of the piezoelectric field, free electrons in the conduction band of ZnO tend to flow and screen the positive ionic piezoelectric charges at one end, leaving the negative ionic piezoelectric charges alone, which reduces the piezoelectric output.[29] As shown in Fig. 3c and d, after the device had been modified with IgG molecules, IgG molecules bind to the Au NP–anti-IgG on the surface of SiO_2/ZnO NWs. An IgG molecule contains four peptide chains (two heavy chains and two light chains), and at the end of the peptide chain are amino groups which are positively charged.[33] The biological receptors (Au NP–anti-IgG) are anchored on the surface of SiO_2/ZnO NWs to recognize target analytes (IgG) through their highly specific binding affinity. When the target is bound by receptors, the surface potential undergoes changes and the carrier density of the conducting channel is modulated through the field effect of the MIS structure.[34] When positively charged IgG molecules bind to the receptor immobilized on an n-type semiconductor channel, the valence (E_V) and conduction (E_C) bands on the surface of ZnO are bent due to the applied charges as a gate potential. Therefore, the distance between the Fermi level (E_F) and the E_C are shifted relatively with the surface potential change. Surrounding positive charges relatively lower the distance between the local E_F and the E_C and increase electron carriers on the surface of the NWs. Thus the positively charged IgG is equivalent to a positive gate potential on the SiO_2/ZnO NWs, and this process can increase the electrons density around the SiO_2/ZnO interfaces. When a compressive force is applied on the device (Fig. 3d), the piezoelectric potential is created along the SiO_2/ZnO NWs, and the increased carrier density around the SiO_2–ZnO interface enhances the screening effect, resulting in the lower piezoelectric output. As SiO_2/ZnO NWs have different electron densities in different concentrations of IgG, the output of the device is affected by electron density contained in the biosensing information. Fig. 3e is a color scale bar that represents the different piezoelectric potential when the device is under a compressive force.

Fig. 4a shows the dependence of the piezoelectric output voltage on the concentration of IgG. The room-temperature piezoelectric output voltage of one device with a size of 3 cm × 3 cm was measured by a low-noise preamplifier under the same applied force (34 N, 0.75 Hz). The enlarged views of the piezoelectric output voltage are shown in Fig. 4b–h. The test number is 10, 9, 10, 8, 10, 10 and 10 with the IgG concentration of 0, 10^{-8}, 10^{-7}, 10^{-6}, 10^{-5}, 10^{-4} and 10^{-3} g mL^{-1}, respectively. The standard deviation (SD) of the piezoelectric output for each concentration of IgG is shown in Fig. 4b–h. When the device is not modified with IgG (Fig. 4b), the piezoelectric output voltage generated by the compressive force is about 0.696 ± 0.0041 V (the relative standard deviation, RSD is 0.59%). After the device had been modified with IgG (Fig. 4c–h), the piezoelectric output decreases due to the increasing electron density induced by the adsorption of positively charged IgG molecules. When the concentration of IgG is 10^{-8}, 10^{-7}, 10^{-6}, 10^{-5}, 10^{-4} and 10^{-3} g mL^{-1}, the piezoelectric output voltage of the device is 0.649 ± 0.0078, 0.583 ± 0.0073, 0.502 ± 0.0119, 0.381 ± 0.0059, 0.250 ± 0.0072 and 0.162 ± 0.0068 V, respectively. The relative standard deviation (RSD) ranges from 1.20% to 4.20%, indicating that the biosensing signal of the device is more stable compared with the bare ZnO device (the RSD ranges from 6.48% to 9.21%).[17] As shown in Fig. 4a, the noise in the measurement is not high compared with the piezoelectric output. The noise arises from the fact that a small amount of SiO_2/ZnO NWs is not vertically aligned on the substrate and the lengths of the NWs are not exactly the same.

The piezoelectric output voltage is linearly dependent on the concentration of IgG (10^{-8}–10^{-3} g mL^{-1}), as shown in Fig. 4i. The calibration curve fits eqn (1):

$$y = a + b \log_{10} x \quad (1)$$

(R^2 = 0.98789, a = −0.14034, b = −0.10029; y is the piezoelectric output voltage, x is the concentration of IgG). The limit of detection (LOD; the signal to noise ratio (SNR) is 3 : 1[35,36]) can be calculated to be about 5.7 ng mL^{-1} by using the fitted linear equation as shown in Fig. 4i. Many other methods have been reported for detecting IgG molecules, such as electrochemical, quartz crystal microbalance (QCM) and surface plasmon resonance (SPR). The comparison of LODs between these methods and our result is shown in Table 1.

The response (a voltage variation in function of the concentration of IgG) of the self-powered/active biosensor can simply be defined as:

$$r\% = \frac{|V_0 - V_i|}{V_0} \times 100\% \quad (2)$$

where V_0 and V_i are the piezoelectric output without IgG and with IgG, respectively. The response (the applied force is 34 N) against 10^{-7}, 10^{-6}, 10^{-5}, 10^{-4} and 10^{-3} g mL^{-1} IgG is about 16.3 ± 1.06, 27.9 ± 1.72, 45.3 ± 0.856, 64.1 ± 1.05 and 76.6 ± 0.987, respectively (shown in Fig. 4j). The sensitivity (the slope of the fitted line in Fig. 4j) can be calculated to be about 14.7. Due to the high affinity of the antigen to antibody, strong reagents are usually used for the dissociation of the complexes.[40,41] Our device is not reusable by using an acid buffer (0.2 M glycine–HCl, pH ~ 2) as the dissociation reagent. The strong acid buffer can damage ZnO NWs, and lower the sensing performance of the device.

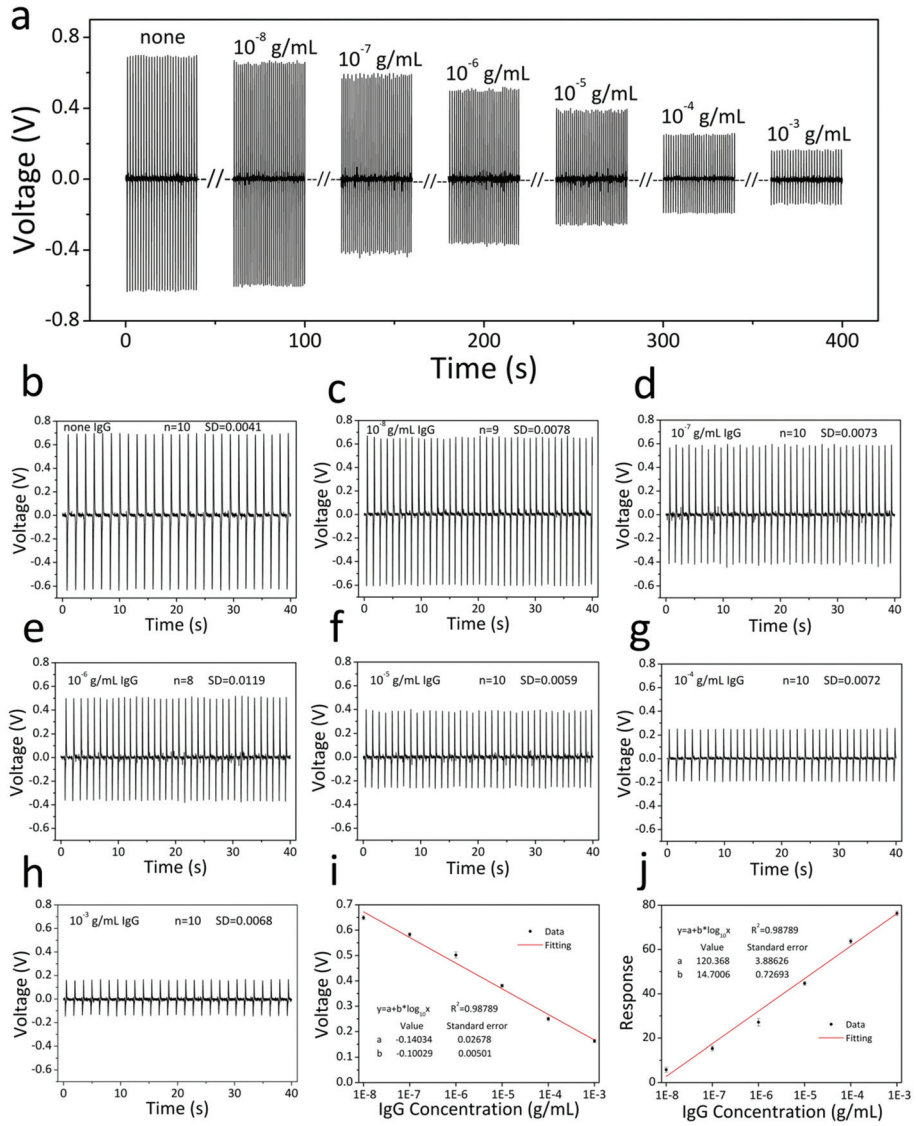

Fig. 4 (a) The piezoelectric output voltage of the device modified with different concentrations of IgG (force = 34 N, 0.75 Hz). (b), (c), (d), (e), (f), (g) and (h) are enlarged views of the piezoelectric output. (i) The relationship between the piezoelectric output of the device and the concentration of IgG. (j) The dependence of the response *r* on the concentration of IgG.

Table 1 The LODs of the different detection methods and the references

Detection method	LOD (ng mL^{-1})	Reference
SiO_2/ZnO self-powered biosensor	5.7	This work
ZnO self-powered biosensor	6.9	17
Electrochemical with microfluidic	10	37
Quartz crystal microbalance	3.5	38
Surface plasmon resonance	7.5	39

Fig. 5a shows the piezoelectric output voltage of the device under different frequency forces, showing that the piezoelectric output voltage is constant with the frequency varying from 0.5 Hz to 2.0 Hz. The piezoelectric output cannot be influenced by the frequency of the force. The relationship between the piezoelectric output voltage and the magnitude of force is shown in Fig. 5b. As the applied force is 18, 22, 26 and 34 N, the piezoelectric output voltage is 0.464, 0.517, 0.569, 0.696 V, respectively. This result indicates that the piezoelectric output voltage can be influenced by the magnitude of the applied force. The piezoelectric output voltage against IgG under different forces (with the same frequency 0.75 Hz) is shown in Fig. 5c–f. As the applied compressive force is 34 N, the piezoelectric output voltage against the IgG concentrations of 0, 10^{-7}, 10^{-6}, 10^{-5}, 10^{-4} and 10^{-3} g mL^{-1} are 0.696 ± 0.0041, 0.583 ± 0.0073, 0.502 ± 0.0119, 0.381 ± 0.0059, 0.250 ± 0.0072 and 0.162 ± 0.0068 V, respectively. When the force is 26 N, the piezoelectric output voltages are 0.569 ± 0.0060, 0.506 ± 0.0069, 0.431 ± 0.0026, 0.334 ± 0.0026, 0.248 ± 0.0043, 0.166 ± 0.0032 V, respectively. When the force is 22 N, the piezoelectric output voltages are 0.517 ± 0.0045, 0.464 ± 0.0029, 0.403 ± 0.0047, 0.313 ± 0.0036, 0.228 ± 0.0035, 0.157 ± 0.0014 V,

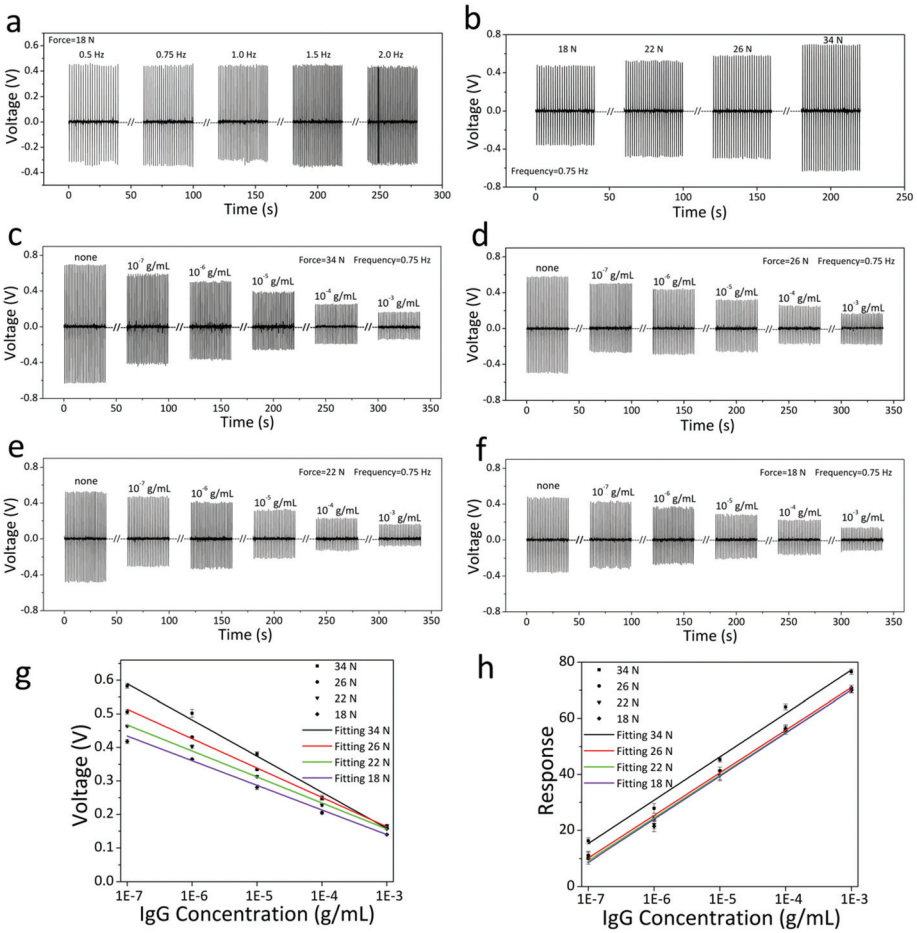

Fig. 5 (a) The piezoelectric output voltage of the device under different frequency forces. (b) The piezoelectric output voltage of the device under different forces. (c), (d), (e) and (f) are the piezoelectric output voltage against the concentration of IgG under different forces (with the same frequency 0.75 Hz). (g) The relationship between the piezoelectric output of the device and the concentration of IgG with a compressive force ranging from 18 to 26 N, respectively. (h) The dependence of the response *r* on the concentration of IgG with a compressive force ranging from 18 to 26 N, respectively.

respectively. When the force is 18 N, the piezoelectric output voltages are 0.465 ± 0.0030, 0.418 ± 0.0062, 0.365 ± 0.0024, 0.280 ± 0.0071, 0.205 ± 0.0044, 0.139 ± 0.0013 V, respectively. Fig. 5g shows the piezoelectric output of the device at different IgG concentrations with the compressive force ranging from 18 to 34 N, showing that the biosensing behavior can be influenced by the applied force. As shown in Fig. 5h, the response of the device against different concentrations of IgG can also be influenced by the applied force. Future work needs to be done to explain this behavior.

It should be pointed that the improvement of the detection limit by coating the SiO_2 layer is a general trend for the self-powered biosensors. The stability of the devices is greatly improved by adding a SiO_2 layer, resulting in enhanced detection limits. In the experiment, we have found that the optimum thickness of the SiO_2 layer ranges from 10 to 20 nm. For the thick SiO_2 layer, although the stability of the device is high, the response is low and could hardly meet the requirement of the practical applications. For the thin SiO_2 layer, the stability is not high (the response is high). Based on our mechanism, the response is the largest when SiO_2 is the thinnest (equivalent to without the SiO_2 layer). For obtaining good detection limit, stability is an important parameter. It should also be noted that other possibilities may exist in the self-powered biosensing process, such as the change of Schottcky barrier height between NWs and contacts due to the absorption of IgG, which can result in the signal change. Thus future work needs to be done to further clarify this piezo-biosensing mechanism and improve the device structure.

The device structure of the SiO_2/ZnO NW biosensor is very flexible making it efficiently convert external compressive strain into an electrical signal. The IgG sensing performance of a device driven by finger bending and releasing is shown in Fig. 6. Fig. 6a shows that the bending and releasing action of the finger can easily deform the flexible device and generate piezoelectricity. Fig. 6b is a schematic image showing the compressive deformation on the device by the finger. The piezoelectric output of the device driven by the finger with 0 and 10^{-3} g mL^{-1} IgG is shown in Fig. 6c, respectively. This result demonstrates the feasible application of this SiO_2/ZnO

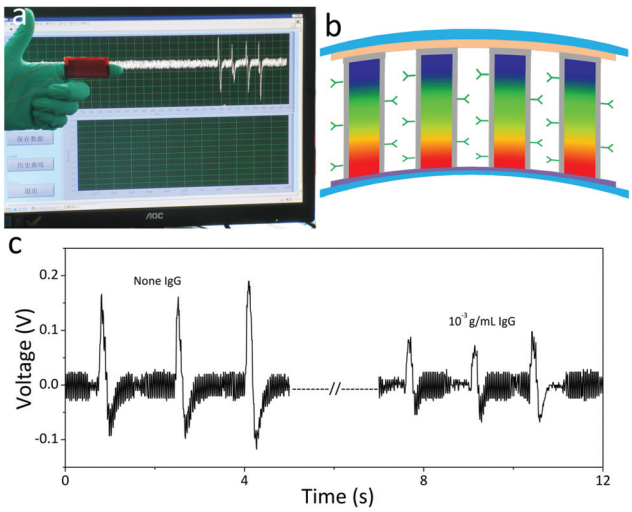

Fig. 6 The piezo-biosensing of the device can be driven by finger bending and releasing. (a) The optical images of the device upon releasing and bending by a finger. (b) Schematic image showing the compressive deformation on the flexible device. (c) The piezoelectric output of the device with 0 and 10^{-3} g mL^{-1} IgG driven by a finger.

NW arrays self-powered/active biosensor in our living environment.

Conclusions

In summary, a highly stable self-powered/active biosensor has been realized from the SiO_2/ZnO NW NG. The relative standard deviation of the device ranges from 1.20% to 4.20%, and the LOD on IgG can reach 5.7 ng mL^{-1}. Introducing a field effect into the self-powered/active biosensing process can greatly improve the sensing performance. Our work can also stimulate a research trend on designing a new device structure and exploring the mechanism for self-powered/active biosensors.

Acknowledgements

This work was supported by the National Natural Science Foundation of China (51102041 and 11104025), the Fundamental Research Funds for the Central Universities (N120205001 and N120405010), and the Program for New Century Excellent Talents in University (NCET-13-0112).

Notes and references

1 R. S. Gaster, D. A. Hall, C. H. Nielsen, S. J. Osterfeld, H. Yu, K. E. Mach, R. J. Wilson, B. Murmann, J. C. Liao, S. S. Gambhir and S. X. Wang, *Nat. Med.*, 2009, **15**, 1327–U1130.
2 L. Shi, Z. Chu, X. Dong, W. Jin and E. Dempsey, *Nanoscale*, 2013, **5**, 10219–10225.
3 N. K. Guimard, N. Gomez and C. E. Schmidt, *Prog. Polym. Sci.*, 2007, **32**, 876–921.
4 Y. Zhao, W. Zhang, Y. Lin and D. Du, *Nanoscale*, 2013, **5**, 1121–1126.
5 L. D. Mello and L. T. Kubota, *Food Chem.*, 2002, **77**, 237–256.
6 J. Xie, X. Jiang, Y. Zhong, Y. Lu, S. Wang, X. Wei, Y. Su and Y. He, *Nanoscale*, 2014, **6**, 9215–9222.
7 P. Lie, J. Liu, Z. Fang, B. Dun and L. Zeng, *Chem. Commun.*, 2012, **48**, 236–238.
8 A. Pandya, P. G. Sutariya, A. Lodha and S. K. Menon, *Nanoscale*, 2013, **5**, 2364–2371.
9 P. Si, P. Kannan, L. Guo, H. Son and D.-H. Kim, *Biosens. Bioelectron.*, 2011, **26**, 3845–3851.
10 J. Lee, S. Choi, S. J. Bae, S. M. Yoon, J. S. Choi and M. Yoon, *Nanoscale*, 2013, **5**, 10275–10282.
11 J. Liu, C. Guo, C. M. Li, Y. Li, Q. Chi, X. Huang, L. Liao and T. Yu, *Electrochem. Commun.*, 2009, **11**, 202–205.
12 M. A. Ibrahem, H.-Y. Wei, M.-H. Tsai, K.-C. Ho, J.-J. Shyue and C. W. Chu, *Sol. Energy Mater. Sol. Cells*, 2013, **108**, 156–163.
13 Z. L. Wang and J. H. Song, *Science*, 2006, **312**, 242–246.
14 S. Xu, Y. Qin, C. Xu, Y. Wei, R. Yang and Z. L. Wang, *Nat. Nanotechnol.*, 2010, **5**, 366–373.
15 R. Zhang, L. Lin, Q. Jing, W. Wu, Y. Zhang, Z. Jiao, L. Yan, R. P. S. Han and Z. L. Wang, *Energy Environ. Sci.*, 2012, **5**, 8528–8533.
16 Y. Lin, P. Deng, Y. Nie, Y. Hu, L. Xing, Y. Zhang and X. Xue, *Nanoscale*, 2014, **6**, 4604–4610.
17 Y. Zhao, P. Deng, Y. Nie, P. Wang, Y. Zhang, L. Xing and X. Xue, *Biosens. Bioelectron.*, 2014, **57**, 269–275.
18 R. Yu, C. Pan, J. Chen, G. Zhu and Z. L. Wang, *Adv. Funct. Mater.*, 2013, **23**, 5868–5874.
19 Z. Li, X. Huang, J. Liu, Y. Li and G. Li, *Mater. Lett.*, 2008, **62**, 1503–1506.
20 H. Cai, C. Xu, P. G. He and Y. Z. Fang, *J. Electroanal. Chem.*, 2001, **510**, 78–85.
21 X. Y. Chen, J. R. Li, X. C. Li and L. Jiang, *Biochem. Biophys. Res. Commun.*, 1998, **245**, 352–355.
22 S. Mao, G. Lu, K. Yu, Z. Bo and J. Chen, *Adv. Mater.*, 2010, **22**, 3521–3526.
23 R. Yu, C. Pan and Z. L. Wang, *Energy Environ. Sci.*, 2013, **6**, 494–499.
24 M. Lee, J. Bae, J. Lee, C.-S. Lee, S. Hong and Z. L. Wang, *Energy Environ. Sci.*, 2011, **4**, 3359–3363.
25 M. W. Allen and S. M. Durbin, *Appl. Phys. Lett.*, 2008, **92**, 122110.
26 J. M. D. Coey, M. Venkatesan and C. B. Fitzgerald, *Nat. Mater.*, 2005, **4**, 173–179.
27 R. Yang, Y. Qin, L. Dai and Z. L. Wang, *Nat. Nanotechnol.*, 2009, **4**, 34–39.
28 C. Pan, Z. Li, W. Guo, J. Zhu and Z. L. Wang, *Angew. Chem., Int. Ed.*, 2011, **50**, 11192–11196.
29 Y. Gao and Z. L. Wang, *Nano Lett.*, 2009, **9**, 1103–1110.
30 Y. Hu, L. Lin, Y. Zhang and Z. L. Wang, *Adv. Mater.*, 2012, **24**, 110–114.

31 Z. L. Wang, *Nano Today*, 2010, **5**, 540–552.
32 Z. L. Wang, *Adv. Mater.*, 2012, **24**, 4632–4646.
33 S. Rosati, R. J. Rose, N. J. Thompson, E. van Duijn, E. Damoc, E. Denisov, A. Makarov and A. J. R. Heck, *Angew. Chem., Int. Ed.*, 2012, **51**, 12992–12996.
34 M.-Y. Shen, B.-R. Li and Y.-K. Li, *Biosens. Bioelectron.*, 2014, **60**, 101–111.
35 J. A. Field and R. L. Reed, *Environ. Sci. Technol.*, 1996, **30**, 3544–3550.
36 F. Toribio, E. Moyano, L. Puignou and M. T. Galceran, *J. Chromatogr. A*, 2002, **948**, 267–281.
37 H. Dong, C.-M. Li, Y.-F. Zhang, X.-D. Cao and Y. Gan, *Lab Chip*, 2007, **7**, 1752–1758.
38 X. Chu, Z. L. Zhao, G. L. Shen and R. Q. Yu, *Sens. Actuators, B*, 2006, **114**, 696–704.
39 Y. Wang, C.-J. Huang, U. Jonas, T. Wei, J. Dostalek and W. Knoll, *Biosens. Bioelectron.*, 2010, **25**, 1663–1668.
40 L. Svobodova, M. Snejdarkova, V. Polohova, I. Grman, P. Rybar and T. Hianik, *Electroanalysis*, 2006, **18**, 1943–1949.
41 M. Liss, B. Petersen, H. Wolf and E. Prohaska, *Anal. Chem.*, 2002, **74**, 4488–4495.

